Giant inverse Rashba-Edelstein effect: Application to monolayer $OsBi_2$

Rui Song,[1,2,3,4] Ning Hao,[3,*] and Ping Zhang[5,2,4,6,†]

[1]*HEDPS, Center for Applied Physics and Technology and School of Physics, Peking University, Beijing 100871, China*
[2]*HEDPS, Center for Applied Physics and Technology and School of Engineering, Peking University, Beijing 100871, China*
[3]*Anhui Key Laboratory of Condensed Matter Physics at Extreme Conditions, High Magnetic Field Laboratory, HFIPS, Anhui, Chinese Academy of Sciences, Hefei, 230031, China*
[4]*Institute of Applied Physics and Computational Mathematics, Beijing 100088, China*
[5]*School of Physics and Physical Engineering, Qufu Normal University, Qufu 273165, China*
[6]*Beijing Computational Science Research Center, Beijing 100084, China*

(Received 11 March 2021; revised 13 September 2021; accepted 16 September 2021; published 29 September 2021)

We propose that the hybridization between two sets of Rashba bands can lead to the unconventional Rashba band structures where the two Fermi circles from different bands own in-plane helical spin textures with the same chiralities, and possess group velocities with the same directions. Through the first-principles calculations, we predict that monolayer $OsBi_2$ hosts such simple and pure unconventional Rashba bands near Fermi energy. Under the weak spin injection, we show that the two Fermi circles from the unconventional Rashba bands both give the positive contributions to the spin-to-charge conversion and thus induce the giant inverse Rashba-Edelstein Effect with large conversion efficiency, which is very different from the conventional Rashba-Edelstein Effect. Our studies not only provide a promising material of monolayer $OsBi_2$ to possess unconventional Rashba bands, but also demonstrate its potential application to achieve highly efficient spin-to-charge conversion in spintronics.

DOI: 10.1103/PhysRevB.104.115433

I. INTRODUCTION

The control and manipulation of the spin-charge interconversion plays a critical role in modern spintronics [1,2]. In the two-dimensional system, the (inverse) Edelstein effect has gained much attention since its potential application in spintronics devices [3–15]. In the direction of inverse Edelstein effect (IEE), a pure spin current j_s through the system generates a transverse charge current j_c, and the Edelstein effect (EE) describes the inverse process. In both cases, the conversion efficiency is defined by $\lambda_{(I)EE} = j_c/j_s$, which largely measures the merits of a physical system.

The microscopic mechanism of both EE and IEE requires the presence of the spin-orbit coupling (SOC), which results in the specific spin-momentum locked electronic band structures. Thus, the usual candidate physical systems include the metallic heterostructure [4–11] and the topological insulators [15–21]. In the metallic heterostructure, the spacial inversion asymmetry lifts the spin degeneracy and gives rise to the Rashba SOC [22]. However, the opposite spin textures of the two lifted bands give the partial compensation of the contributions to the spin-to-charge conversion and suppresses the efficiency λ_{IEE} [15], and searching for materials with strong Rashba SOC coupling becomes an alternative way to increase λ_{IEE} in this situation [23–29]. Furthermore, the interfacial effects complicate the descriptions of the electronic states beyond the standard Rashba model and limit the application of the metallic heterostructure. In the topological insulator, the topological surface state possesses the single Dirac cone structure, which can get rid of of partial compensation effect in Rashba system [15]. However, the concurrence of surface and bulk states and quantum confinement effect always complicate TI-based systems beyond the controllability [30].

In this work, we propose the third kind of system, which provides a new way to achieve the giant IEE with large λ_{IEE}. The new system has two spin-lifted bands with the identical spin textures, i.e., unconventional Rashba bands, which is very different from the conventional Rashba bands with opposite spin textures. We first perform the first-principles calculations to predict a simple compound of monolayer $OsBi_2$, which hosts simple and pure unconventional Rashba band structures near Fermi energy. We further construct an effective $k \cdot p$ Hamiltonian to describe such unconventional Rashba bands. According to the semiclassical Boltzmann transport theory, we show that the unconventional Rashba bands can induce strongly enhanced spin-to-charge conversion and possess the giant IEE with large λ_{IEE}. The calculated spin-to-charge conversion efficiency λ_{IEE} is estimated to be about ten times that of the conventional Rashba system. It is worth noting that the pure bulk states of a single material can overcome the shortcomings of the complexity and fragility of the interfacial and surface states in the metallic heterostructure and topological insulators. These properties make monolayer $OsBi_2$ to be a promising material to realize the giant IEE and to have potential application in spintronics.

This paper is organized as follows. First, we discuss the difference between the conventional and unconventional Rashba bands and construct the effective model to describe the uncon-

*haon@hmfl.ac.cn
†zhang_ping@iapcm.ac.cn

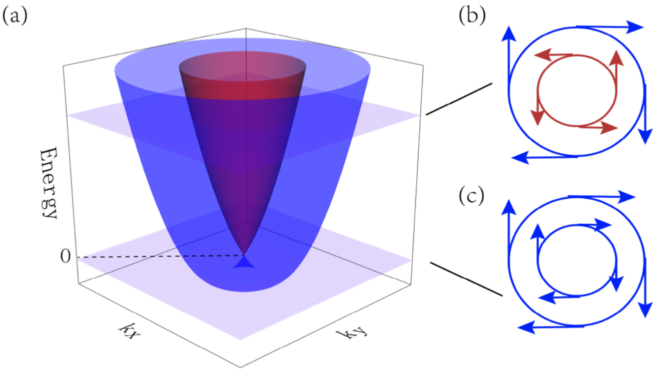

FIG. 1. (a) The conventional Rashba band structure. (b) and (c) The spin textures of two Fermi circles when Fermi energy $E_F > 0$ and $E_F < 0$, respectively.

ventional Rashba bands in monolayer $OsBi_2$ in Sec. II. Next, we calculate and find the giant giant IEE according to the semiclassical Boltzmann transport theory in Sec. III. At last, we discuss the experimental feasibility to realize the giant IEE with monolayer $OsBi_2$, and give the conclusions.

II. THE UNCONVENTIONAL RASHBA BANDS IN MONOLAYER $OsBi_2$

We start with the conventional Rashba bands described by $E_{\pm}(k) = \varepsilon \mathbf{k}^2 \pm \alpha_R|\mathbf{k}|$ with ε and α_R the constant and Rashba SOC parameters, respectively. The two outer and inner bands and the Fermi contour involving two Fermi circles for a specific Fermi energy E_F are shown in Fig. 1. The spin textures of the two Fermi circles are denoted by the red and blue arrows, as shown in Fig. 1(b) and 1(c). In the case of Fermi energy $E_F > 0$, the two Fermi circles have spin textures with opposite chiralities and group velocities $\mathbf{v}_F^{\pm} = \frac{1}{\hbar}\nabla_{\mathbf{k}} E_{\pm}(k)|_{\mathbf{k}=\mathbf{k}_F^{\pm}}$ with the same directions, as shown in Fig. 1(b). For $E_F < 0$, the two Fermi circles are from the same outer band $E_-(k)$, and they have the spin textures with same chiralities but group velocities $\mathbf{v}_F^-$ with opposite directions, as shown in Fig. 1(c). When the spin current is injected, the opposite chiral spin textures in the former case and the opposite directions of the velocities in the latter case can both suppress the converted charge current, because the two Fermi circles give a partial compensation for the contributions to the converted charge current [15]. This is the key reason to limit the spin-to-charge conversion efficiency λ_{IEE} in conventional Rashba system. To break the bottleneck, a natural strategy is to force both Fermi circles to have positive contributions to spin-to-charge conversion. Namely, both Fermi circles have spin textures with the same chiralities and the group velocities with the same directions. Such unconventional Rashba band structures were experimentally observed in some surface alloy systems such as Bi/Cu(111), $BiAg_2$/Ag-Au(111) and was argued to originate from the hybridizations between different bands and orbitals [31–34]. However, the complicated and fragile band structures limit the possibility of exploring the spin-charge interconversion efficiency in these systems.

To overcome the complexity from the coexistence of both unconventional Rashba bands and other trivial bands in metallic heterostructure, we search for the single compound with the pure and robust unconventional Rashba bands near Fermi energy. Our previous studies indicate that the trigonal layered $PtBi_2$-type materials tend to form the buckled structure for the top layer of Bi [35]. Such kind of distortion naturally breaks the inversion symmetry. Following the similar strategy, we perform the first-principles calculations to search for the compounds with same structures but different elements. Namely, the $PtBi_2$-type compounds have crystallographic expression AB_2 with A and B taking (Ru, Os, Rh, Pt, Pd, Ir) and B taking (Sb, Pd, Sn, Bi), respectively. We find that only monolayer $OsBi_2$ is unique to meet all the requirements and to possess the simple and pure unconventional Rashba bands near Fermi energy. The relaxed structure is shown in Fig. 2(a) and 2(b). The crystal constant is $a = b = 6.78$ Å. The calculated band structure is shown in Fig. 2(c) and 2(d). The point group is C_{3v} for monolayer $OsBi_2$. Without SOC, the two-fold degenerate points at Γ point belong to the two-dimensional irreducible representations (IRs) labeled by E, as shown in Fig. 2(c). There exist two such E points around Fermi energy with one and another mainly involving (d_{xz}, d_{yz}) and $(d_{xy}, d_{x^2-y^2})$ orbitals of Os, respectively. When SOC is tuned on, each E IR is doubled and split into one two-dimensional Γ_4 IR and two one-dimensional Γ_5 and Γ_6 IRs [36]. Deviate from Γ point, the two sets of Γ_4 bands split into Rashba-type and further couple together to give the unconventional spin textures, as conformed by Fig. 2(e).

The effective $k \cdot p$ Hamiltonian $H(k)$ near Γ point can be constructed under the basis defined by $\Gamma_4 \oplus \Gamma_4$. The explicit form of $H(k)$ is restricted by C_{3v} point group symmetry and time-reversal (TR) symmetry. Namely, $D(\hat{g})H(k)D^{-1}(\hat{g}) = H(\hat{g}k)$ and $\hat{T}^{-1}H_c(k)\hat{T} = H_c(-k)$. Here, $\hat{g}$ is the symmetry operation of C_{3v} point group, $D(\hat{g})$ is the matrix representation of $\hat{g}$, and $\hat{T}$ is TR operator. For C_{3v} point group, there are two group generators which are rotating $\frac{2\pi}{3}$ around z-axis and reflecting by the three vertical mirrors. Applying these restrictions on $H(k)$, we obtain $H(k)$ up to the k-quadric terms as follows (see Supplemental Material) [37]:

$$H(k) = A(k) + \begin{pmatrix} B(k) & i\alpha_R k_- & 0 & \beta k_- \\ -i\alpha_R k_+ & B(k) & \beta k_+ & 0 \\ 0 & \beta k_- & -B(k) & i\alpha_R k_- \\ \beta k_+ & 0 & -i\alpha_R k_+ & -B(k) \end{pmatrix}. \tag{1}$$

Here, $A(k) = \gamma k^2 + \gamma_0$, $B(k) = \delta k^2 + \delta_0$, and $k_{\pm} = k_x \pm ik_y$. By fitting the parameters to the first-principles calculations, we obtain $\gamma = -8.5\,\text{eV}\text{Å}^2$, $\gamma_0 = 0.24\,\text{eV}$, $\delta = -0.4\,\text{eV}\text{Å}^2$, $\delta_0 = 0.08\,\text{eV}$, $\alpha_R = 0.78\,\text{eV}\text{Å}$, and $\beta = 1.26\,\text{eV}\text{Å}$. The fitting bands are indicated by the red-dashed lines shown in Fig. 2(d).

III. THE GIANT INVERSE RASHBA-EDELSTEIN EFFECT IN MONOLAYER $OsBi_2$

Now, we consider the spin-to-charge conversion of the bands from Hamiltonian in Eq. (1). For convenience, we redefine $\varepsilon = \gamma + \delta$, $\varepsilon_0 = \gamma_0 + \delta_0$, $\varepsilon' = \gamma - \delta$, $\varepsilon'_0 = \gamma_0 - \delta_0$. In order to perform the analytic calculation, we further approximately adopt $\varepsilon' = \varepsilon$ and make $\varepsilon'_0 = 0$ through tuning the chemical potential. The parameters ε, ε_0, ε', and ε'_0 are

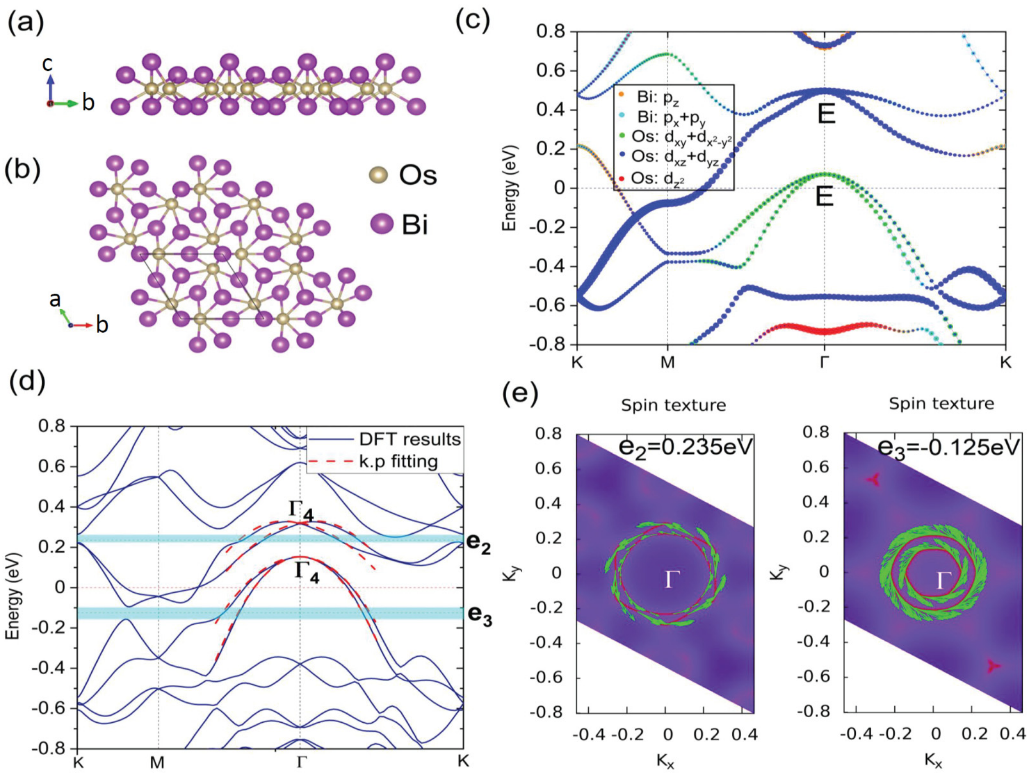

FIG. 2. (a) and (b) The top and side view of the Crystal structure of monolayer $OsBi_2$, respectively. (c) The orbital-resolved band structures along the high-symmetry lines without spin-orbit coupling. (d) The band structures along the high-symmetry lines with spin-orbit couplings. The red-dashed lines label the fitting bands from the effective k · p Hamiltonian. (e) The spin textures of different Fermi circles around Γ point for two different Fermi energy 0.235eV and −0.125eV, respectively. The green arrows indicate the direction and intensity of spin textures.

recovered to describe the bands of $OsBi_2$ when numerical calculations are performed. For $\varepsilon < 0$ and $\varepsilon_0 > 0$, the band structures are schematically shown in Fig. 3. Consider a couple of inner and outer Fermi circles from the two lower-energy bands as shown in Fig. 3(b), the spin textures can be evaluated by $\mathbf{S}_{\mathbf{k}}^{\pm} = \langle \Psi_{\pm}(\mathbf{k})|\mathbf{\Omega}|\Psi_{\pm}(\mathbf{k})\rangle$. $\mathbf{\Omega} = \tau_0 \otimes \boldsymbol{\sigma}$, with τ_0 and $\boldsymbol{\sigma}$ spanning the orbital and spin space. Then,

$$\mathbf{S}_{\mathbf{k}}^{+} = \frac{2\alpha_R k - \varepsilon_0}{\sqrt{(2\alpha_R k - \varepsilon_0)^2 + \beta^2 k^2}}(\sin\theta\hat{\mathbf{x}} - \cos\theta\hat{\mathbf{y}}), \tag{2}$$

$$\mathbf{S}_{\mathbf{k}}^{-} = \frac{2\alpha_R k + \varepsilon_0}{\sqrt{(2\alpha_R k + \varepsilon_0)^2 + \beta^2 k^2}}(\sin\theta\hat{\mathbf{x}} - \cos\theta\hat{\mathbf{y}}), \tag{3}$$

according to which, three regions can be divided by different fillings. Region I is from $E_{\max}$ to E_D, where the two Fermi circles is from the single outer band and have the same chiral spin textures, as shown in Fig. 3(c). Region II is from E_D to E_c with $E_c = E^{\text{outer}}(k_c)$ and $k_c = \frac{\varepsilon_0}{2\alpha_R}$. In region II, the two Fermi circles possess opposite chiral spin textures, as shown in in Fig. 3(d). Region III is from E_c to negative infinity, where the two Fermi circles share the same chiral spin textures, as shown in in Fig. 3(e). More remarkably, two Fermi circles in Region III have the same directions of velocities. This means the band structures in the Region III belong to the unconventional Rashba-type. The situations are similar for the two higher-energy bands in Fig. 3(b).

When spin is injected into the system along **z** direction, as shown in Fig. 3(f), the two Fermi circles in Region III should move $\delta\mathbf{k}$ along the same direction in momentum space, as shown in Fig. 3(g) and 3(h). Such Fermi circles shift means the in-plane charge current is generated. This is the physical picture of the spin-to-charge conversion, i.e., the IEE. In the semiclassical Boltzmann transport theory [52], the shift of the Fermi circles is equivalent to application of a homogeneous electrostatic field **E**, which generates a directional current and makes the distribution function f_k to deviate from the equilibrium distribution function f_k^0. In the zero-temperature limit, we have $f_k = f_k^0 - |e|\mathbf{\Lambda}_{\boldsymbol{k}} \cdot \mathbf{E}\, \delta(E_k - E_F)$, and the spin polarization $\langle \mathbf{S}\rangle$ can be expressed as $\langle \mathbf{S}\rangle = \sum_k \mathbf{S}_k(f_k - f_k^0)$. Here, e is the elementary charge, and $\mathbf{\Lambda}_{\boldsymbol{k}}$ is the mean free path. Under the relaxation-time approximation, $\mathbf{\Lambda}_{\boldsymbol{k}} = \tau_k \mathbf{v}_k$ with τ_k and $\mathbf{v}_k$ the momentum relaxation time and the group velocity, respectively. We consider two Fermi circles from two lower-energy bands, as shown in Fig. 3(b). Note that the results for two Fermi circles from two higher-energy bands are similar. With the help of the spin textures in Eqs. (2) and (3) [37], we have

$$\langle \mathbf{S}\rangle = \frac{|e|A}{2\pi\hbar}\sum_{\eta} I^{\eta}\left(k_F^{\eta}\right)\tau_F^{\eta}k_F^{\eta}\left(\hat{\mathbf{v}}_F^{\eta}\cdot\hat{\mathbf{k}}_F^{\eta}\right)(\hat{\mathbf{z}}\times\mathbf{E}). \tag{4}$$

Here, $\eta = \pm$ labels the inner and outer Fermi circles, respectively. $I^{\eta}(k) = (2\alpha_R k + \eta\varepsilon_0)/\sqrt{(2\alpha_R k + \eta\varepsilon_0)^2 + \beta^2 k^2}$ is the factor for spin polarization. A, $\hat{\mathbf{v}}_F$ and $\hat{\mathbf{k}}_F$ is the area of the unit cell, the unit vector of group velocity and Fermi momentum, respectively. Since the two Fermi circles share identical directions of spin polarization and group velocity in Region III, they both give positive contributions to total

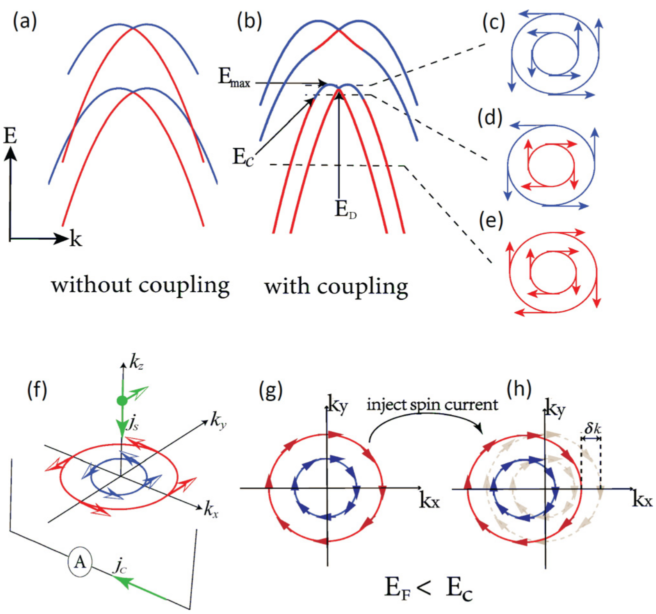

FIG. 3. (a) and (b) The two sets of Rashba bands without and with couplings, respectively. E_D labels the cross point of two bands. (c), (d), and (e) The spin textures for the two Fermi circles from the two lower-energy bands, when the Fermi energy E_F lies in Region I, II and III, respectively. (f) The schematic diagram for the spin-to-charge conversion through the unconventional Rashba band structure shown in (c), i.e., IEE. The $\hat{z}$-directional spin current j_s with $\hat{y}$-directional spin polarization can generates $\hat{x}$-directional charge current j_c. (g) and (h) The configurations of the two Fermi circles from two higher-energy bands shown in (c) before and after injection of spin current, respectively.

spin polarization. Additionally, as shown in Fig. 4(a), the rate of interband scattering is greatly reduced with the decrease of E_F, because the spin-flip backscattering is forbidden. Accordingly, the momentum relaxation time τ_k is also increased. These two aspects strongly enhance the spin polarization $\langle\mathbf{S}\rangle$, as shown in Fig. 4(b). When $E_F \ll E_c$, the factor of spin polarization and radii of two Fermi circles tend to be equal, the spin polarization can be approximately expressed as

$$\langle\mathbf{S}\rangle_{E_F\gg E_c} = \frac{\alpha_R|e|}{2\pi N_{\rm im}V_0^2}\left(\sqrt{1+\frac{4\varepsilon\Delta E_F}{\alpha_R^2+\beta^2}}-1\right)(\hat{\mathbf{z}}\times\mathbf{E}) \qquad (5)$$

with $\Delta E_F = E_F - \frac{1}{2}\varepsilon_0$. Here, $N_{\rm im}$ and V_0 denote the number of δ-scattering centers and the s-wave scattering potential, respectively. In conventional Rashba system, the spin polarization [37] $\langle\mathbf{S}\rangle_{\rm Rashba} = \alpha_R|e|/(2\pi N_{\rm im}V_0^2)$, which is a constant when $E_F < 0$. Thus, the spin polarization in unconventional Rashba system rapidly surpasses the conventional one, as shown in Fig. 4(b).

The spin current density $\mathbf{j}_s$ shown in Fig. 4(c) can be related with the spin polarization $\langle\mathbf{S}\rangle$ shown in Eq. (4) by $\mathbf{j}_s = \frac{e\langle S\rangle}{\tau_F}\hat{\mathbf{z}}$. The generated charge current density $\mathbf{j}_c$ shown in Fig. 4(c) can be obtained by $\mathbf{j}_c = e\sum_k \mathbf{v}_k(f_k - f_k^0)$. The spin-to-charge conversion efficiency λ_{IEE} can be further expressed as

$$\lambda_{IEE} = j_c/j_s = \frac{\sum_\eta k_F^\eta\tau_F^\eta v_F^\eta}{\sum_\eta I^\eta(k_F^\eta)k_F^\eta(\hat{\mathbf{v}}_F^\eta\cdot\hat{\mathbf{k}}_F^\eta)}. \qquad (6)$$

For the conventional Rashba system, $\lambda_{\rm IEE}^{\rm con} \sim \alpha_R\tau_F/\hbar + 4\varepsilon\tau_F E_F/(\alpha_R\hbar)$ with a nearly constant τ_F. Then, $\lambda_{\rm IEE}^{\rm con}$ tends to be the constant λ_0, when $E_F \sim 0$, and is linearly increased with the shift of E_F, indicated by the blue line in Fig. 4(d). For the unconventional Rashba system, however, with the increase of E_F, the interband scattering rate $\propto |\langle\Psi_+(k)|\Psi_-(k)\rangle|^2$ rapidly decreases, as shown in Fig. 4(a), which gives a large momentum-relaxation time τ_F. Thus, the larger charge current j_c is generated. Meanwhile, stronger spin polarization generates larger spin current j_s. These two effects compete with each other. The numerical results of the relative j_c and j_s for monolayer $OsBi_2$ are shown in Fig. 4(c), from which, one can clearly find the competitive relation between j_c and j_s. Compared with conventional Rashba system, monolayer $OsBi_2$ has lower rate of increase but much larger initial value of λ_{IEE} length, as indicated by the red curve in Fig. 4(d). In the energy window we most concern, such as the shadowed regions in Fig. 4(d), the monolayer $OsBi_2$ has $\lambda_{\rm IEE}^{\rm uncon}/\lambda_{\rm IEE}^{\rm con} \sim 10$. Its $\lambda_{\rm IEE}^{\rm uncon}/\lambda_{\rm IEE}^{\rm con}$ could be up to 16 when $\lambda_{\rm IEE}^{\rm con}$ approximately takes the constant $\alpha_R\tau_F/\hbar$, which is usually adopted in many literatures [5,15,28]. The monolayer $OsBi_2$ with unconventional Rashba bands has remarkable advantages than conventional Rashba systems.

IV. DISCUSSIONS AND CONCLUSIONS

Note that the aforementioned discussions focus on either the two higher-energy bands or the two lower-energy bands, as shown in Figs. 2(d) and 3(b). In the continuous model described by Eq. (1), all four bands should be considered. However, in monolayer $OsBi_2$, the lattice symmetries force only two bands to be occupied and the other two bands to be gapped when the Fermi energy lies in the shadowed regions, as shown in Fig. 2(c). Unlike monolayer $OsBi_2$, the two higher-energy bands and the two lower-energy bands cannot be separated in metallic heterostructure such as Bi/Cu(111) and $BiAg_2$ /Ag-Au(111) [31–34]. This is a crucial point to guarantee monolayer $OsBi_2$ not metallic heterostructures to realize the giant IEE.

To test the stability and practicability of $OsBi_2$, we perform the first-principles calculations to calculate the phonon spectrum and do the *ab initio* molecular dynamics simulation to estimate energy evolution [37]. We find that there is no imaginary frequency of the phonon spectrum [37]. We adopt a relatively large supercell consisting of 4×4 repeated unit cells to simulate the lattice. After heating at 300 K for 12 ps with a time step of 2 fs, we find no structure reconstruction and the corresponding fluctuation of energy (temperature) with time are negligible [37]. These results indicate the structure of $OsBi_2$ is stable. We further take into account the Hubbard interaction U up to 3 eV, and find the band renormalization is negligible [37]. The reason is due to the weakly correlated interaction of unfilled 5d orbitals of Os. It is worth noting that the $PtBi_2$ has been experimentally exfoliated into a monolayer due to the weak interlayer van der Waals interaction [51]. We also calculate the exfoliation energy of $PtBi_2$ and $OsBi_2$, and find that the exfoliation energy of $OsBi_2$ is even lower than that of PtBi [37]. It indicates the feasibility to prepare the monolayer $OsBi_2$ from the bulk compound.

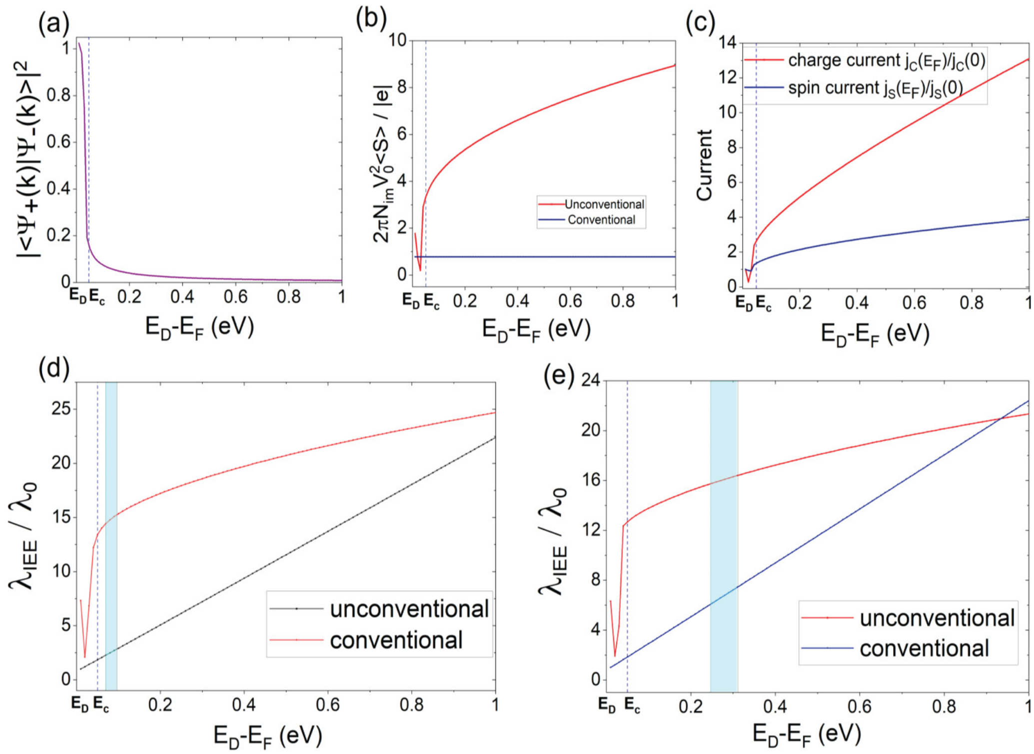

FIG. 4. (a) The interband scattering factor $|\langle\Psi_+(k)|\Psi_-(k)\rangle|^2$ as function as Fermi energy. (b) Total spin polarization of conventional and unconventional Rashba systems, where we adopt the same parameter of Rashba coupling α_R. (c) The relative spin current $j_s(E_F)/j_s(0)$ and the relative charge current $j_c(E_F)/j_c(0)$ as the function as the Fermi energy for the unconventional Rashba systems. (d) and (e) The spin-to-charge conversion efficiency λ_{IEE} of the conventional and unconventional Rashba systems as the function as the Fermi energy. Here, λ_{IEE} is in unit of λ_0, which is the IEE length of conventional Rashba system at $E_F = 0$. The shadowed regions correspond to the shadowed regions shown in Fig. 2(d). Note that the fitting parameters for monolayer $OsBi_2$ are adopted in the numerical calculations of (a)–(e). (a)–(c) are the numerical results for the two lower-energy bands shown in Fig. 2(d), and the relevant results for the two higher-energy bands are shown in Fig. 7 in Ref. [37].

In practice, the monolayer $OsBi_2$ should be sustained by a substrate and covered by a capping layer to block the air. If the sample is prepared with epitaxial method, we propose a sandwich structure $Sc_2O_3/Os(Bi_{1-x}Pb_x)_2/Sc_2O_3$, and calculate the bands of this sandwich structure. We find that the hybridization between $Os(Bi_{1-x}Pb_x)_2$ and Sc_2O_3 is negligible around the Femi level, because Sc_2O_3 is a good insulator with a gap about 4 eV [37]. Thus, the unconventional Rashba bands are well preserved as the free standing case. The Fermi level can be tuned by introducing hole-type carriers, i.e., $Sc_2O_3/Os(Bi_{1-x}Pb_x)_2/Sc_2O_3$. Our calculation shows $x = 0.09$ corresponds to dope 0.54 hole/unit cell, and the Fermi level shifts down and lies in the shadowed region in Fig. 2(b) [37]. Note that similar chemical doping has been experimentally realized in $Pt_{1-x}Rh_xBi_2$ [53]. Besides, other practical methods can be adopted, such as electrostatic gating and ionic liquid gating, etc. [54–60].

In conclusion, we propose that the unconventional Rashba system provides a new way to realize the spin-to-charge conversion. Our first-principles calculations prove that monolayer $OsBi_2$ host such simple, pure and robust unconventional Rashba bands. With the help of semiclassical transport theoretical analysis, we find that the spin-to-charge conversion efficiency of monolayer $OsBi_2$ is much higher than that in the conventional Rashba system. These results make monolayer $OsBi_2$ to be a promising material to host the giant IEE. Our studies provide a new path to promote the charge-to-spin conversion efficiency in modern spintronics.

ACKNOWLEDGMENTS

This work was financially supported by the National Key R&D Program of China No. 2017YFA0303201, National Natural Science Foundation of China under Grants (No. 12022413, 11674331, No.11625415), the "Strategic Priority Research Program (B)" of the Chinese Academy of Sciences, Grant No. XDB33030100, the '100 Talents Project' of the Chinese Academy of Sciences, the Collaborative Innovation Program of Hefei Science Center, CAS (Grants No. 2020HSC-CIP002), the CASHIPS Director's Fund (BJPY2019B03), the Science Challenge Project under Grant No. TZ2016001. A portion of this work was supported by the High Magnetic Field Laboratory of Anhui Province, China.

[1] J. Sinova, S. O. Valenzuela, J. Wunderlich, C. H. Back, and T. Jungwirth, Rev. Mod. Phys. **87**, 1213 (2015).

[2] I. Žutić, J. Fabian, and S. Das Sarma, Rev. Mod. Phys. **76**, 323 (2004).

[3] V. M. Edelstein, Solid State Commun. **73**, 233 (1990).
[4] C. R. Ast, J. Henk, A. Ernst, L. Moreschini, M. C. Falub, D. Pacilé, P. Bruno, K. Kern, and M. Grioni, Phys. Rev. Lett. **98**, 186807 (2007).
[5] J. C. Rojas-Sanchez, L. Vila, G. Desfonds, S. Gambarelli, J. P. Attane, J. M. D. Teresa, C. Magen, and A. Fert, Nat. Commun. **4**, 2944 (2013).
[6] S. Sangiao, J. M. D. Teresa, L. Morellon, I. Lucas, M. C. Martinez-Valarte, and M. Viret, Appl. Phys. Lett. **106**, 172403 (2015).
[7] A. Nomura, T. Tashiro, H. Nakayama, and K. Ando, Appl. Phys. Lett. **106**, 212403 (2015).
[8] M. B. Jungfleisch, W. Zhang, J. Sklenar, W. Jiang, J. E. Pearson, J. B. Ketterson, and A. Hoffmann, Phys. Rev. B **93**, 224419 (2016).
[9] M. Isasa, M. C. Martínez-Valarte, E. Villamor, C. Magén, L. Morellón, J. M. De Teresa, M. R. Ibarra, G. Vignale, E. V. Chulkov, E. E. Krasovskii, L. E. Hueso, and F. Casanova, Phys. Rev. B **93**, 014420 (2016).
[10] H. J. Zhang, S. Yamamoto, B. Gu, H. Li, M. Maekawa, Y. Fukaya, and A. Kawasuso, Phys. Rev. Lett. **114**, 166602 (2015).
[11] H. Nakayama, Y. Kanno, H. An, T. Tashiro, S. Haku, A. Nomura, and K. Ando, Phys. Rev. Lett. **117**, 116602 (2016).
[12] M. Offidani, M. Milletari, R. Raimondi, and A. Ferreira, Phys. Rev. Lett. **119**, 196801 (2017).
[13] L. A. Beníez, W. S. Torres, J. F. Sierra, M. Timmermans, J. H. Garcia, S. Roche, M. V. Costache, and S. O. Valenzuela, Nat. Mater. **19**, 170 (2020).
[14] E. Lesne, Y. Fu, S. Oyarzun, J. C. Rojas-Sánchez, D. C. Vaz, H. Naganuma, G. Sicoli, J.-P. Attané M. Jamet, E. Jacquet, J.-M. George, A. Barthélémy, H. Jaffrès, A. Fert, M. Bibes, and L. Vila, Nat. Mater. **15**, 1261 (2016).
[15] J.-C. Rojas-Sánchez, S. Oyarzún, Y. Fu, A. Marty, C. Vergnaud, S. Gambarelli, L. Vila, M. Jamet, Y. Ohtsubo, A. Taleb-Ibrahimi, P. Le Fèvre, F. Bertran, N. Reyren, J.-M. George, and A. Fert, Phys. Rev. Lett. **116**, 096602 (2016).
[16] L. Fu, C. L. Kane, and E. J. Mele, Phys. Rev. Lett. **98**, 106803 (2007).
[17] L. Fu and C. L. Kane, Phys. Rev. B **76**, 045302 (2007).
[18] M. Z. Hasan and C. L. Kane, Rev. Mod. Phys. **82**, 3045 (2010).
[19] X.-L. Qi and S.-C. Zhang, Rev. Mod. Phys. **83**, 1057 (2011).
[20] M. Rodriguez-Vega, G. Schwiete, J. Sinova, and E. Rossi, Phys. Rev. B **96**, 235419 (2017).
[21] R. Dey, N. Prasad, L. F. Register, and S. K. Banerjee, Phys. Rev. B **97**, 174406 (2018).
[22] Y. A. Bychkov and E. I. Rashba, J. Phys. C **17**, 6039 (1984).
[23] K. Ishizaka, M. S. Bahramy, H. Murakawa, M. Sakano, T. Shimojima, T. Sonobe, K. Koizumi, S. Shin, H. Miyahara, A. Kimura, K. Miyamoto, T. Okuda, H. Namatame, M. Taniguchi, R. Arita, N. Nagaosa, K. Kobayashi, Y. Murakami, R. Kumai, Y. Kaneko *et al.* Nat. Mater. **10**, 521 (2011).
[24] J. Park, S. W. Jung, M.-C. Jung, H. Yamane, N. Kosugi, and H. W. Yeom, Phys. Rev. Lett. **110**, 036801 (2013).
[25] A. Varykhalov, D. Marchenko, M. R. Scholz, E. D. L. Rienks, T. K. Kim, G. Bihlmayer, J. Sánchez-Barriga, and O. Rader, Phys. Rev. Lett. **108**, 066804 (2012).
[26] D. Niesner, M. Wilhelm, I. Levchuk, A. Osvet, S. Shrestha, M. Batentschuk, C. Brabec, and T. Fauster, Phys. Rev. Lett. **117**, 126401 (2016).
[27] A. Crepaldi, L. Moreschini, G. Autes, C. Tournier-Colletta, S. Moser, N. Virk, H. Berger, Ph. Bugnon, Y. J. Chang, K. Kern, A. Bostwick, E. Rotenberg, O. V. Yazyev, and M. Grioni, Phys. Rev. Lett. **109**, 096803 (2012).
[28] K. Shen, G. Vignale, and R. Raimondi, Phys. Rev. Lett. **112**, 096601 (2014).
[29] A. Johansson, J. Henk, and I. Mertig, Phys. Rev. B **93**, 195440 (2016).
[30] M. S. Bahramy, P. D. C. King, A. de la Torre, J. Chang, M. Shi, L. Patthey, G. Balakrishnan, Ph. Hofmann, R. Arita, N. Nagaosa, and F. Baumberger, Nat. Commun. **3**, 1159 (2012).
[31] H. Mirhosseini, J. Henk, A. Ernst, S. Ostanin, C.-T. Chiang, P. Yu, A. Winkelmann, and J. Kirschner, Phys. Rev. B **79**, 245428 (2009).
[32] C. Mera Acosta, O. Babilonia, L. Abdalla, and A. Fazzio, Phys. Rev. B **94**, 041302(R) (2016).
[33] I. A. Nechaev and E. E. Krasovskii, Phys. Rev. B **100**, 115432 (2019).
[34] H. Bentmann, S. Abdelouahed, M. Mulazzi, J. Henk, and F. Reinert, Phys. Rev. Lett. **108**, 196801 (2012).
[35] W. Gao, X. Zhu, F. Zheng, M. Wu, J. Zhang, C. Xi, P. Zhang, Y. Zhang, N. Hao, W. Ning M. Tian, Nat. Commun. **9**, 3249 (2018).
[36] G. F. Koster, *Properties of the Thirty-Two Point Groups* (MIT Press, Cambridge, MA, 1963), Vol. 24.
[37] See Supplemental Material at http://link.aps.org/supplemental/10.1103/PhysRevB.104.115433 for details about the first-principles calculating methods, derivation of the effective Hamiltonian, the warping effect of the spin textures, the spin textures of the coupled Rashba bands in other conditions, the calculations of spin polarization, spin current density and charge current density (see also Refs. [29,38–51] therein).
[38] G. Kresse and J. Furthmüller, Phys. Rev. B **54**, 11169 (1996).
[39] G. Kresse and D. Joubert, Phys. Rev. B **59**, 1758 (1999).
[40] P. E. Blochl, Phys. Rev. B **50**, 17953 (1994).
[41] J. P. Perdew, K. Burke, and M. Ernzerhof, Phys. Rev. Lett. **77**, 3865 (1996).
[42] A. Togo, L. Chaput, and I. Tanaka, Phys. Rev. B **91**, 094306 (2015).
[43] Q. Wu, S. Zhang, H.-F. Song, M. Troyer, and A. A. Soluyanov, Comput. Phys. Commun. **224**, 405 (2018).
[44] A. A. Mostofi, J. R. Yates, G. Pizzi, Y.-S. Lee, I. Souza, D. Vanderbilt, and N. Marzari, Comput. Phys. Commun. **185**, 2309 (2014).
[45] L. Bellaiche and D. Vanderbilt, Phys. Rev. B **61**, 7877 (2000).
[46] C. Eckhardt, K. Hummer, and G. Kresse, Phys. Rev. B **89**, 165201 (2014).
[47] C.-X. Liu, X.-L. Qi, HaiJun Zhang, X. Dai, Z. Fang, and S.-C. Zhang, Phys. Rev. B **82**, 045122 (2010).
[48] L. Fu, Phys. Rev. Lett. **103**, 266801 (2009).
[49] Z. Alpichshev, J. G. Analytis, J.-H. Chu, I. R. Fisher, Y. L. Chen, Z. X. Shen, A. Fang, and A. Kapitulnik, Phys. Rev. Lett. **104**, 016401 (2010).
[50] Z. Li and J. P. Carbotte, Phys. Rev. B **89**, 165420 (2014).
[51] X.-A. Nie, S. Li, M. Yang, Z. Zhu, H.-K. Xu, X. Yang, F. Zheng, D. Guan, S. Wang, Y.-Y. Li, C. Liu, J. Li, P. Zhang, Y. Shi, H. Zheng, and J. Jia, ACS Nano **14**, 2366 (2020).
[52] I. Mertig, Rep. Prog. Phys. **62**, 237 (1999).
[53] G. Shipunov, I. Kovalchuk, B. R. Piening, V. Labracherie, A. Veyrat, D. Wolf, A. Lubk, S. Subakti, R. Giraud, J. Dufouleur,

S. Shokri, F. Caglieris, C. Hess, D. V. Efremov, B. Büchner, and S. Aswartham, Phys. Rev. Mater. **4**, 124202 (2020).
[54] L. J. Li, E. C. T. O'Farrell, K. P. Loh, G. Eda, B. Özyilmaz, and A. H. Castro Neto, Nature (London) **529**, 185 (2016).
[55] Y. Saito, T. Nojima, and Y. Iwasa, Supercond. Sci. Technol. **29**, 093001 (2016).
[56] K. Ueno, S. Nakamura, H. Shimotani, A. Ohtomo, N. Kimura, T. Nojima, H. Aoki, Y. Iwasa, and M. Kawasaki, Nat. Mater. **7**, 855 (2008).
[57] J. M. Lu, O. Zheliuk, I. Leermakers, N. F. Q. Yuan, U. Zeitler, K. T. Law, and J. T. Ye, Science **350**, 1353 (2015).
[58] D. Costanzo, S. Jo, and H. Berger, Nat. Nanotechnol. **11**, 339 (2016).
[59] E. Sajadi, T. Palomaki, Z. Fei, W. Zhao, P. Bement, C. Olsen, S. Luescher, X. D. Xu, J. A. Folk, and D. H. Cobden, Science **362**, 922 (2018).
[60] V. Fatemi, S. F. Wu, Y. Cao, L. Bretheau, Q. D. Gibson, K. Watanabe, T. Taniguchi, T. J. Cava, and P. Jarillo-Herrero, Science **362**, 926 (2018).